DOI: 10.61782/fa.2023.0413

forum acusticum 2023

ASSESSMENT OF ELECTRIC POWERTRAIN WHINING NOISE CONTRIBUTION UNDER EARLY-STAGE DESIGN UNCERTAINTIES

Vinay PRAKASH[1,2*] **Olivier SAUVAGE**[1] **Jérôme ANTONI**[2]
Laurent GAGLIARDINI[1]
[1] Stellantis N.V., 2 boulevard de l'Europe, 78300 Poissy, France
[2] Univ Lyon, INSA Lyon, LVA, EA677, 69621 Villeurbanne, France

ABSTRACT

Despite the advantage of being quieter than traditional internal combustion engine vehicles, electric vehicles are often distinguished by high-frequency tonal components, which can be perceived as unpleasant to the occupants. To ensure optimal acoustic comfort in electric vehicles, it is important to analyze the NVH behavior of e-powertrains during the early stages of the design process which poses inherent uncertainties, such as varying operating conditions, partial knowledge of design parameters, dispersion in measurement data, etc. To effectively address these uncertainties, it is necessary to use fast and comprehensive stochastic models during the design phase. In this work, a deterministic framework is first presented to estimate the e-powertrain's interior whining noises combining both airborne & structure-borne contribution. Subsequently, under probabilistic framework, the uncertainties are introduced in the deterministic models considering random sampling of operating conditions, and the chosen geometrical design parameters for the e-machine under assessment. A multivariate Bayesian metamodel helps to incorporate prior knowledge on the uncertain parameters and generate the posterior distribution of harmonic forces. The uncertainties in sound pressure level are propagated through weakly-coupled multi-physical domains estimated using semi-analytical approaches and combined with measured vehicle transfer functions. Sensitivity analysis using the developed metamodel provides an efficient way to reinstate prior beliefs about the unknown parameters.

Keywords: *NVH, electric motor, probabilistic models, Bayesian approaches, uncertainty quantification, meta-models*

1. INTRODUCTION

Noise, vibration and harshness (NVH) is one of the key criteria that significantly affects customer's perception of quality and an overall image of the vehicle. Due to the absence of ICE, BEVs are much quieter but have a different acoustic signature. The interior noise contribution has high-frequency tonal components (also known as whining noise) that are usually perceived as rather annoying and unpleasant to the occupants [1]. The major sources of interior noise in EVs can still be broadly classified under three categories namely, aerodynamic noise, tire-pavement interaction noise, and e-powertrain noise. The first two contributions make up the background (or masking) noise and the main source of whining (tonal) comes from the electrified powertrains. The whining noise along with the background masking can be combined to produce a key performance indicator, for instance, prominence ratio. A generic flowchart is shown in Figure 1, considering three major noise sources discussed above dependent globally on the operating conditions or the client-driving profiles.

There has been a considerable level of research done to estimate e-powertrain's acoustic performance (ref [2] and [3]). However, most of the studies in the past have

*Corresponding author: vinay.prakash@stellantis.com

approached the problem considering either a deterministic setting for the operating conditions and design architectures or focusing only on the local acoustic performance of e-motors without considering the different transfer paths leading to the interior cabin noise. As shown in [4], Bayesian surrogates (or metamodels) can be developed from masking noise measurement data (dashed blue box in Figure 1) utilizing the prior-domain knowledge resulting in the uncertainty estimates of the resulting interior sound pressure level (SPL). These probabilistic metamodels are easy-to-evaluate functional mappings where the desired response is a distribution of probable outputs instead of a single point-estimate. The focus of this article is to build probabilistic surrogates for the electromagnetic whine shown in the dashed red box in Figure 1 and will be detailed in the next subsection.

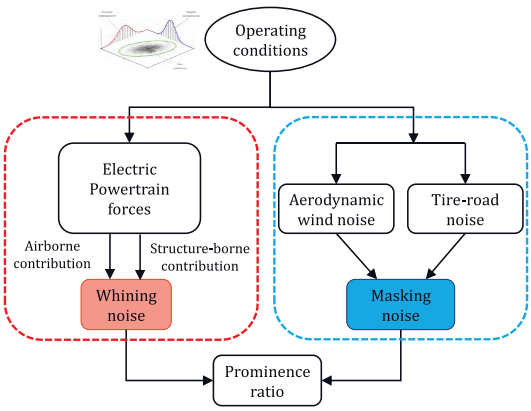

Figure 1. Flow chart of the global noise generation mechanism in BEVs

Scope: In this study, interior-PMSM (IPMSM) is used in which the permanent magnets are embedded in the rotor core. The mechanical (for e.g., gear whine) and aerodynamic noises are not considered for the sake of simplicity, but the same methodological framework applies. In addition, since the structure-borne contribution is more challenging than airborne, it will be the focus of this study. Besides, global surrogates are modeled within Bayesian framework to account for the uncertainty in whining noise prediction for EVs during early-stage NVH design. Moreover, the sources of uncertainties considered in this work are the uncertainties arising from variable operating conditions and the partial-knowledge on e-machine architecture and control parameters during early-stage design.

2. PROBLEM DESCRIPTION

Focusing only on the dashed red box in Figure 1, the whining noise assessment due to electromagnetic interaction within IPMSMs involves an interplay between different weakly-coupled physical mechanisms as shown in Figure 2. For an efficient propagation of uncertainties, two stochastic metamodels are developed: one for electromagnetic forces under 'e-motor stage', and second for powertrain suspension under 'vehicle stage'.

The real-life client driving profiles are represented as pairs of $(\boldsymbol{\Omega}, \boldsymbol{\tau})$ with $\boldsymbol{\Omega}$ being the motor speed in [RPM] and $\boldsymbol{\tau}$ being the wheel torque in [Nm]. $\boldsymbol{\mathcal{P}}_{\mathrm{OC}} \subseteq \mathbb{R}^{N_s \times 2}$ is a set containing N_s samples of such operating conditions (OC) sampled randomly from the joint-pdf available *a-priori*. The set of geometrical parameters are represented as $\boldsymbol{\mathcal{P}}_{\mathrm{geo}} \subseteq \mathbb{R}^{N_s \times n_{\mathrm{geo}}}$, where n_{geo} is the number of design parameters considered and $\boldsymbol{\mathcal{P}}_{\mathrm{control}} \subseteq \mathbb{R}^{N_s \times 2}$ is the set of control parameters in pairs of $(\boldsymbol{I}, \boldsymbol{\phi})$, where $\boldsymbol{I}$ is the root-mean-square amplitude of the current and $\boldsymbol{\phi}$ is its phase angle in electrical degree.

Under deterministic setting i.e., for a particular input parameter set (with $N_s = 1$), the 2D EM domain is solved considering 1/8$^{\mathrm{th}}$ sector of the full-model (shown in Figure 3) using the open-source tool FEMM coupled with Pyleecan [5]. The Maxwell pressure, hereafter referred to as the airgap surface force (AGSF) in [N/m^2] [6], is computed along the middle of the airgap in both radial and tangential directions. Let r be the spatial order of the force with respect to the tooth angle in the stator frame θ which determines the periodic shape of the force distribution, and s be the electrical order with respect to the angular frequency $\omega_e = 2\pi f_e$ with $f_e = \frac{\Omega}{60} N_{\mathrm{pp}}$, where N_{pp} is the number of pole-pairs in the nominal design. In this article, a progressive wave of spatial order r and frequency f_e is denoted by a pair (r, sf_e). The mechanical frequency is given by, $f_{\mathrm{mech}} = \frac{\Omega}{60}$ [Hz] and the mechanical orders will be denoted by, $k_{\mathrm{mech}} = sN_{\mathrm{pp}}$. For instance, Figure 4 shows the radial component of the AGSF at $\Omega = 495$ RPM along dominant spatial and mechanical orders. These excitations are usually mapped on to the structural domain using commercially available FE codes (see [2] and [7]). However, in this work, a semi-analytical approach is investigated and therefore, the dynamic response of the IPMSM to the EM excitation is computed analytically by considering a thin cylindrical shell representative of the simplified stator-system. Then, the natural frequencies of the stator system can be approximately given by [8]:

$$f_{mn}^{\text{stat}} \approx \frac{1}{2\pi}\sqrt{\frac{K_m^{\text{core}} + K_{mn}^{\text{frame}} + K_m^{\text{winding}}}{M^{\text{core}} + M^{\text{frame}} + M^{\text{winding}}}} \quad (1)$$

where, $m \in \{0,1,..,N_m\}, n \in \{1,..,N_n\}$ denote the circumferential and axial nodes of the simplified cylindrical system, respectively and $\boldsymbol{K}, \boldsymbol{M}$ represent the calculated stiffness [N/m] and mass [kg] of each subsystem, respectively.

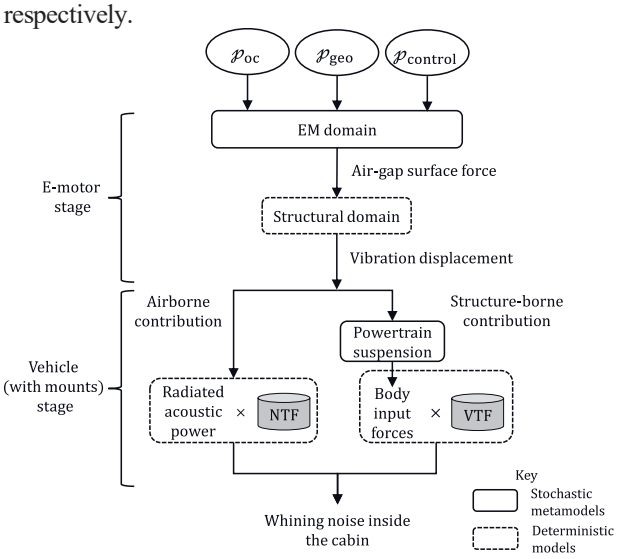

Figure 2: Overview of the multi-physical mechanism involved in the generation of whining noise in BEVs (EM: electromagnetic, NTF: noise transfer function, VTF: vibration transfer function)

The root-mean-squared (RMS) vibration displacement on the motor surface is estimated through finite number of spatial modes as in modal expansion. The axial modal function and the corresponding participating factors are determined as per [9] and [10]. For airborne contribution, the equation for radiated power is readily available, refer [8]. In structure-borne path, the RMS vibration displacement from the motor surface exerts force on the vehicle body through powertrain mounting systems. This input force on the vehicle body is identified using a Stellantis internally developed MATLAB tool based on lumped parameters that acts as a transfer function when provided with unit displacement at the outer surface of the motor. The true RMS vibration can then be coupled with this transfer function to get the recomposed body-input force. To get the interior cabin SPL due to structure-borne mechanism, the recomposed body-input force is coupled with the available measured VTF.

Under stochastic setting, the desired output is the pdf of the SPL inside the cabin due to uncertain OCs, uncertain design and control parameters.

In this work, Bayesian hierarchical models are developed that encode the probabilistic dependencies between the random variables. Each unknown parameter in the model is considered as a random variable that follows a prior-pdf characterized by its own hyper-parameters. These hyper-parameters incorporate the objective prior-knowledge available through domain expertise. Based on Bayes' theorem, the posterior distribution of the unknown parameters is approximated using Monte Carlo methods [11].

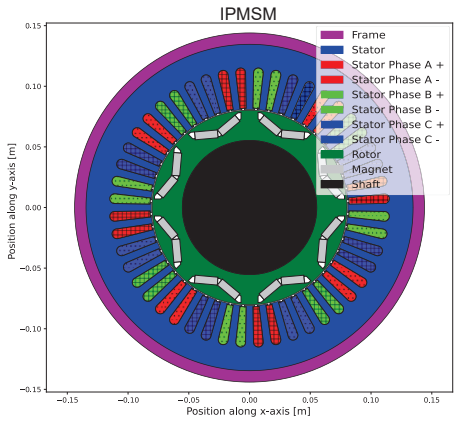

Figure 3: Nominal IPMSM design considered as an example use-case

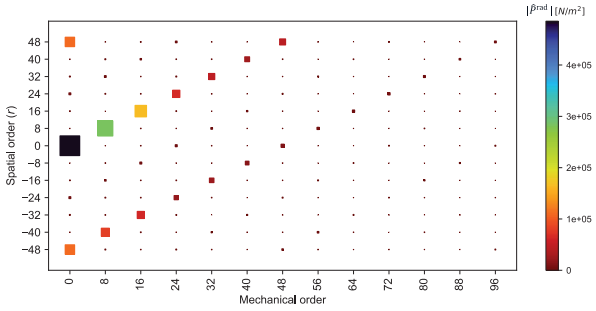

Figure 4: Radial AGSF component at 495 RPM

Let $\boldsymbol{X}^{\text{train}}, \boldsymbol{y}^{\text{train}}$ be the training input parameters and the observed output responses, respectively. Then, the full-posterior pdf of the unknown random parameters $\boldsymbol{\theta}$ is given by:

$$p(\boldsymbol{\theta}|\boldsymbol{y}^{\text{train}}, \boldsymbol{X}^{\text{train}}, \mathcal{M}) \propto f(\boldsymbol{y}^{\text{train}}|\boldsymbol{\theta}, \boldsymbol{X}^{\text{train}}, \mathcal{M})p(\boldsymbol{\theta}) \quad (2)$$

where, $f(\boldsymbol{y}^{\text{train}}|\boldsymbol{\theta}, \boldsymbol{X}^{\text{train}}, \mathcal{M})$ is the likelihood function dependent on the parameters of the model, $p(\boldsymbol{\theta})$ is the prior pdf on the unknown random parameters and $\mathcal{M}$ is the model specification.

The process of Bayesian predictive metamodeling can then be divided into two stages where, in the first stage [12], the unknown parameters of the model are trained based on the observed/simulated data, and in the second stage on the basis of new input data ($\tilde{\boldsymbol{X}}$), the samples are drawn from the posterior predictive distribution given by,

$$p(\tilde{\boldsymbol{y}}|\boldsymbol{y}^{\text{train}}, \tilde{\boldsymbol{X}}, \boldsymbol{\theta}, \mathcal{M}) = \int p(\tilde{\boldsymbol{y}}|\boldsymbol{\theta})\, p(\boldsymbol{\theta}|\boldsymbol{y}^{\text{train}}, \tilde{\boldsymbol{X}}, \mathcal{M}) \mathrm{d}\boldsymbol{\theta} \quad (3)$$

which gives the predictive distribution on the new input set given the observed training data.

3. PROBABILISTIC METAMODEL FOR AGSF ($\mathcal{M}^{\text{AGSF}}$)

3.1 Data generation

For the training stage, let $\mathfrak{D}^{\text{train}} = \{(\boldsymbol{x}_i, \boldsymbol{y}_i)\}_{i=1}^{N_s}$ be the training dataset, such that $\boldsymbol{x}_i \in \boldsymbol{X}^{\text{train}} \subseteq \mathbb{R}^{N_s \times N_p}$, and $\boldsymbol{y}_i \in \boldsymbol{Y}^{\text{train}} \subseteq \mathbb{R}^{N_s \times N_r}$, where N_r is the total number of frequency bins corresponding to a pair (r, sf_e). The operating conditions are sampled using the inverse-transform sampling from the joint-pdf of (Ω, τ) and the joint kernel density estimate (kde) of the samples can be seen in Figure 5. Other input parameters (design and control) are supposed to follow inverse gamma distributions whose support is $(0, \infty)$.

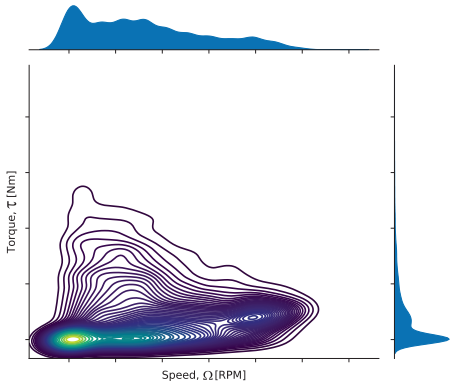

Figure 5: Joint distribution of the sampled OCs ($\boldsymbol{\Omega}, \boldsymbol{\tau}$). The two shaded curves at the edges represent the marginal distribution of the respective variable

It is to note that under steady-state conditions, the AGSF does not depend on Ω and therefore, variable operating speed only influences the spatial frequencies at which AGSF acts. For $N_s = 100$ at $\Omega = 495$ RPM, the dominant combined (radial and tangential) AGSF is shown in Figure 6.

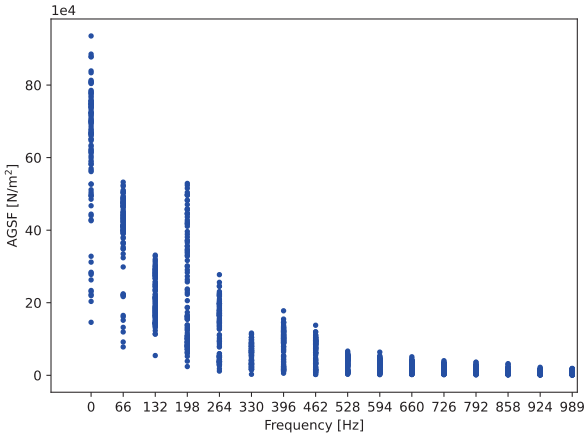

Figure 6: AGSF output from 100 input training parameters

3.2 Hierarchical model training stage

Once the training data is available, the Bayesian model can be formulated. In this work, it is assumed that the observed data ($\boldsymbol{y}^{\text{train}}$) is distributed as per the Normal distribution with mean ($\boldsymbol{\mu}_y$) and variance ($\boldsymbol{\sigma}_y^2$). Also, heteroscedasticity in the observed data is considered i.e., the variance of the responses varies along the space of input predictor variables. The Bayesian hierarchical model for training stage is shown in Figure 7, where it can be seen that $\boldsymbol{X}^{\text{train}}, \boldsymbol{Y}^{\text{train}}$ are the observed variables and the stochasticity is considered only in the model coefficients and the variance.

Each observed training data ($\boldsymbol{y}_i(\omega) \in \mathbb{R}^{1 \times N_r}$) can be represented as:

$$\boldsymbol{y}_i(\omega) = f_i(\boldsymbol{x}, \boldsymbol{\alpha}) + \boldsymbol{\eta} \quad (4)$$

$$f_i(\boldsymbol{x}, \boldsymbol{\alpha}) = \boldsymbol{\alpha}_0 + \sum_{j=1}^{n_j} \boldsymbol{\alpha}_j \boldsymbol{x}_i^{\odot j} \quad (5)$$

where, $\boldsymbol{x}_i \in \mathbb{R}^{n_p \times 1}$ is the predictor vector, $\odot$ represents the Hadamard power where each element in $\boldsymbol{x}$ raised to power j, $\boldsymbol{\alpha}_0 \in \mathbb{R}^{1 \times N_r}, \boldsymbol{\alpha}_j \in \mathbb{R}^{N_r \times n_p}$ are the vectors of unknown coefficients, $\boldsymbol{\eta} \in \mathbb{R}^{1 \times N_r}$ is the vector of fitting errors consisting of modelling errors and is assumed as a zero mean Gaussian noise with variance $\boldsymbol{\sigma}_y^2$, n_j is the degree of the polynomial, and $f_i(\boldsymbol{x}, \boldsymbol{\alpha})$ represents the surrogate function. For N_s training samples, the multivariate polynomial regression model can be formulated as:

$$\boldsymbol{y}^{\text{train}} = \widehat{\boldsymbol{X}}\boldsymbol{\theta} + \boldsymbol{\eta} \quad (6)$$

where, $\widehat{\boldsymbol{X}} = [\mathbf{1}\ \boldsymbol{X}^{\text{train}}\ (\boldsymbol{X}^{\text{train}})^{\odot 2}\ \dots\ (\boldsymbol{X}^{\text{train}})^{\odot n_j}] \in \mathbb{R}^{N_s \times (n_j n_p + 1)}$ is the augmented predictor matrix and $\boldsymbol{\theta} = [\boldsymbol{\alpha}_0\ \boldsymbol{\alpha}_1\ \boldsymbol{\alpha}_2\ \dots\ \boldsymbol{\alpha}_{n_j}] \in \mathbb{R}^{(n_j n_p + 1) \times N_r}$ is the matrix containing the unknown coefficients.

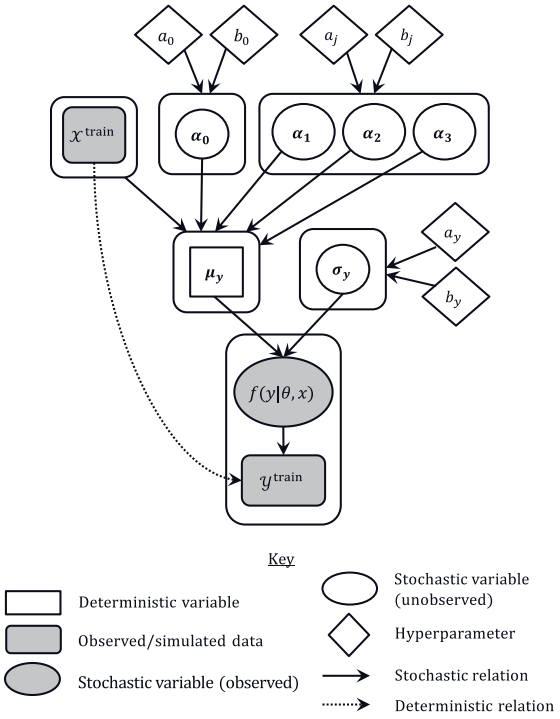

Figure 7: Training stage hierarchical Bayesian model

The Bayesian model during the training stage is written as:

$$\boldsymbol{y}^{\text{train}} | \boldsymbol{X}^{\text{train}}, \boldsymbol{\theta}, \boldsymbol{\eta} \sim \mathcal{N}(\widehat{\boldsymbol{X}}\boldsymbol{\theta}, \boldsymbol{\sigma}_y^2) \quad (7)$$

$$\boldsymbol{\alpha}_0 \sim \mathcal{N}(\boldsymbol{\mu}_0, \boldsymbol{\sigma}_0^2) \quad (8)$$

$$\boldsymbol{\alpha}_j \sim \mathcal{N}(\boldsymbol{\mu}_j, \boldsymbol{\sigma}_j^2), \forall j = 1, \dots, n_j \quad (9)$$

$$\boldsymbol{\sigma}_y^2 \sim \text{InvGamma}(\boldsymbol{a}_y, \boldsymbol{b}_y) \quad (10)$$

The presented model is built in Python framework using open-source PyMC3 library [13]. A total of 4 different MCMC chains were simulated resulting in 8,000 samples. The burn-in sample size (samples that are typically discarded during MCMC sampling, refer [11]) was set to 1,000 for each chain.

3.3 Bayesian model evaluation

To evaluate the developed Bayesian model, different diagnostics are developed (see [13]). One such widely used is Gelman-Rubin statistic, given by $\hat{R}$ (should ideally be equal to 1.0) which measures the ratio of inter-chains and intra-chain variances. For all the unknown parameters in the developed Bayesian model, $\hat{R} = 1.0$. Another intuitive way of diagnosing the model is to replicate the data and then overlay its distribution on the distribution of the originally observed data. If the model is well-specified, the posterior predictive replicated samples must have a similar distribution as the observed data. This can be seen in Figure 8, where the kde of 100 samples is similar to the kde of $\boldsymbol{y}^{\text{train}}$.

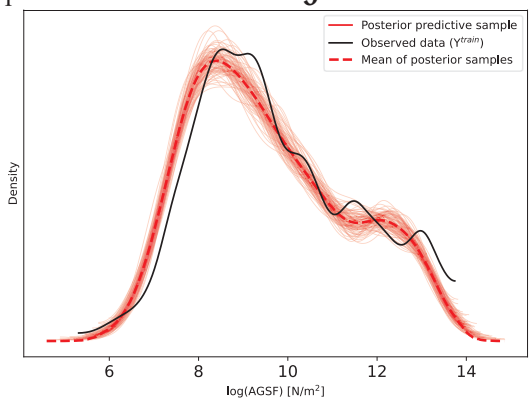

Figure 8: Posterior predictive check with $\boldsymbol{X}^{\text{train}}$

3.4 Bayesian metamodel exploitation stage

Based on the input data ($\widetilde{\boldsymbol{X}}$) as per analyst's knowledge and need (by specifying the distribution's hyper-parameters), the posterior predictive samples are generated from the trained model using Eqn. [3] and the drawn samples can be seen in Figure 9. The uncertainty estimates can be plotted using a Box-and-whisker plot describing the spread and the median of the data with quartiles. It is clear that the inter-quartile range varies across the spatial frequencies and is mostly higher for orders greater than 16 (or equivalently, $f \geq 198$ Hz). Therefore, considering the prior sampling distribution of input parameters, the variability (or pdf, by taking the kde) of AGSF can be described at discrete spatial frequencies.

A typical metamodel exploitation scheme for AGSF is shown in Figure 10. The uncertainty from AGSF posterior samples is combined with uncertain mass of each subsystem ($M^{\text{subsystem}}$) and the natural frequencies to produce uncertain RMS vibration displacements at the surface of the IPMSM.

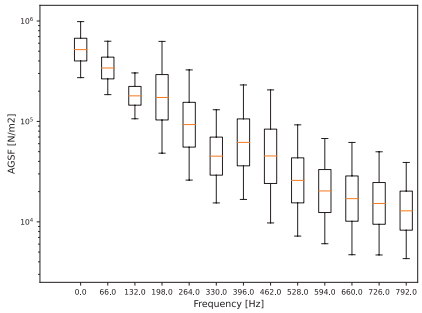

Figure 9: AGSF posterior predictive samples with new input parameters $\tilde{\boldsymbol{X}}$

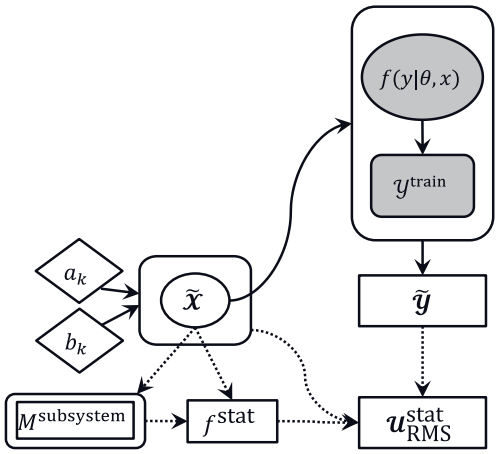

Figure 10: Metamodel exploitation stage with $\tilde{\boldsymbol{X}}$ (Key to identify different elements in the scheme remains same as used in Figure 7)

4. PROBABILISTIC METAMODEL FOR POWERTRAIN SUSPENSION ($\mathcal{M}^{\text{sus}}$)

In structure-borne noise transmission to the interior cabin, the vibration displacement at the motor surface is transmitted to the vehicle-body through the mounting system. Considering 3-point suspension architecture, as shown in Figure 11, the total input degrees of freedom (dofs) is 9 corresponding to the vibration response at 3 mounts and in 3 directions $(\boldsymbol{x}, \boldsymbol{y}, \boldsymbol{z})$. As mentioned before, an internal Stellantis tool has been used to estimate the transfer function resulting in the force acting on the vehicle-body when provided with the unit displacement on each mount and in each direction.

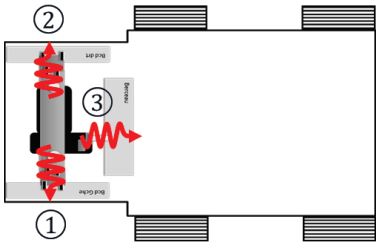

Figure 11: A typical 3-point e-powertrain suspension architecture (1: left mount connection to the vehicle-body, 2: right mount connection, 3: connection to the cradle point)

To consider stochasticity in the mounting behaviour, the position coordinates and stiffness parameters of the rubber mounts are considered random. A similar Bayesian scheme is implemented as shown the previous subsection for training the model. The posterior predictive distribution of the resulting transfer function ($\boldsymbol{H}_{\text{MB}}$) from left mount to the vehicle-body in x-direction at a particular spatial order $r = 8$ is shown in Figure 12.

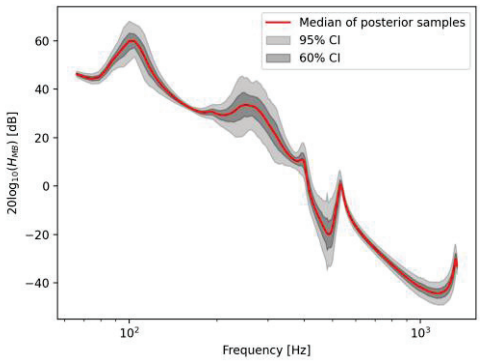

Figure 12: Posterior predictive distribution of transfer function (CI stands for credible interval)

5. COMBINING TWO METAMODELS

The posterior samples of uncertain RMS vibration displacement from the first metamodel ($\mathcal{M}^{\text{AGSF}}$) is then coupled with the posterior samples of uncertain transfer function from powertrain suspension metamodel ($\mathcal{M}^{\text{sus}}$).

The flowchart of the steps is shown in Figure 13. The recomposed force acting on the car-body ($\boldsymbol{F}^{\mathrm{cb}}$) is given by,

$$\boldsymbol{F}^{\mathrm{cb}}_{i,j}(\boldsymbol{\omega}) = \boldsymbol{H}^{i}_{MB}(\omega) \circ \boldsymbol{\mathcal{U}}^{j}_{\mathrm{RMS}}(\omega), \quad i,j \in \{1,2,\dots,N_{\mathrm{post}}\} \tag{11}$$

where, N_{post} is the number of posterior samples drawn from each metamodel, and $\circ$ denote the Hadamard product between vectors.

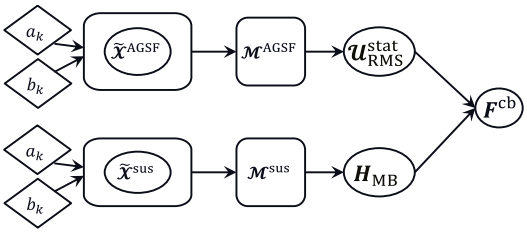

Figure 13: Flowchart describing the coupling of two metamodels to get the input carbody force ($\boldsymbol{F}^{\mathbf{cb}}$)

The recomposed uncertain input carbody force is then coupled with the available measured VTF to get the SPL inside the cabin. The frequency range for the measurement was [20,2048] Hz and the response was recorded for multiple location inside the cabin (two front left seat, two back left seat, etc.). In this study, the mean of front left seat measurements was considered. The interior SPL through left mount in all directions along with the quadratic average of these contributions can be seen in Figure 14. The variability in the SPL is due to the uncertainties introduced in OCs, macro geometrical parameters and control parameters. The same approach can be repeated for each mount and in each direction. Needless to say, the metamodel $\mathcal{M}^{\mathrm{sus}}$ is expected to perform quick computations as it must be trained for each dof and for different spatial orders. However, when the frequency resolution is excessively high, the training duration using the current multivariate polynomial method remains ineffective. Nevertheless, data reduction techniques can be employed on the output space and then a similar approach can be employed to reduce the training time, which will be a part of future work.

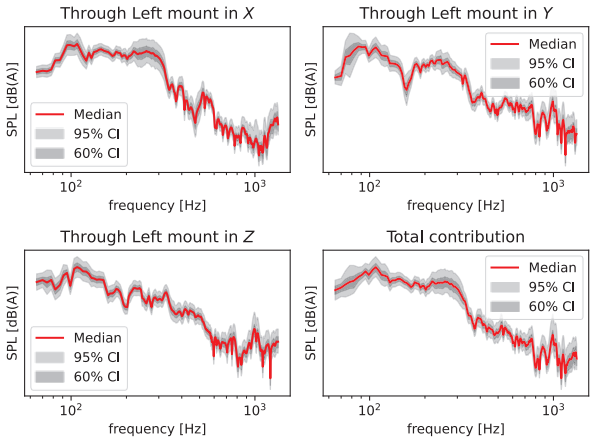

Figure 14: Interior SPL through left mount for spatial order 8

6. CONCLUSIONS & PERSPECTIVES

During the early-stage vehicle design, under insufficient information regarding various parameters and architectures, deterministic approach is no longer useful, and the resulting uncertainties can be modelled through Bayesian approach which considers the prior-domain knowledge combined with available data. In this work, a two-stage Bayesian metamodel is developed from simplified semi-analytical models and applied to the structure-borne contribution of e-powertrains to the interior SPL. In addition, it was shown that multiple metamodels can be used to efficiently propagate uncertainties coming from OCs, design and control parameters. Hence, under the partial knowledge of the complex system made up of several subsystems, an estimate of the uncertainty on the output responses can be obtained with the presented methodology.

For perspectives, indeed, uncertainties coming from the available measured data could also be considered along with efficient data reduction techniques improving the performance of metamodel training stage. A comprehensive metamodel would then include not just the estimates from structure-borne contribution but also from airborne contribution. Moreover, such metamodels would allow to perform efficient sensitivity analysis to infer information about the most influential parameters.

7. ACKNOWLEDGMENTS

This research work is funded by the European Commission's H2020-Innovative training network (ITN) under the project ECODRIVE (Grant Nr. 858018) and we gratefully acknowledge the support of OpenLab Vibro-Acoustic-Tribology@Lyon, Laboratoire Vibrations Acoustique (LVA), INSA Lyon and the NVH department of Stellantis N.V.

8. REFERENCES

[1] Qian, K., Wang, J., Gao, Y., Sun, Q., and Liang, J., "Interior noise and vibration prediction of permanent magnet synchronous motor," *Journal of Vibroengineering* 20(5):2225–2236, 2018.

[2] Deng, W. and Zuo, S., "Electromagnetic Vibration and Noise of the Permanent-Magnet Synchronous Motors for Electric Vehicles: An Overview," *IEEE Trans. Transp. Electrific.* 5(1):59–70, 2019, doi:10.1109/TTE.2018.2875481.

[3] Vijayraghavan, P., "Noise in Electric Machines: A Review," *IEEE Transactions on industry applications* 35(5):8, 1999.

[4] Prakash, V., Sauvage, O., Antoni, J., and Gagliardini, L., "Bayesian NVH metamodels to assess interior cabin noise using measurement databases," *Proceedings of the 30th International Conference on Noise and Vibration Engineering, ISMA*, 1666–1684, 2022

[5] Bonneel, P., Le Besnerais, J., Pile, R., and Devillers, E., "Pyleecan: an open-source Python object-oriented software for the multiphysic design optimization of electrical machines," *2018 XIII International Conference on Electrical Machines (ICEM)*, IEEE, ISBN 1-5386-2477-X: 948–954, 2018

[6] Pellerey, Pierre. "Étude et optimisation du comportement vibro-acoustique des machines électriques: application au domaine automobile." PhD diss., Compiègne, 2012.

[7] Dupont, J.-B., Bouvet, P., and Wojtowicki, J.-L., "Simulation of the airborne and structure-borne noise of electric powertrain: Validation of the simulation methodology," SAE Technical Paper, ISBN 0148-7191: 2013-01–2005, 2013.

[8] Gieras, J.F., Wang, C., and Lai, J.C., "Noise of polyphase electric motors," CRC press, ISBN 1-315-22098-9, 2018

[9] Blevins, R.D. and Plunkett, R., "Formulas for natural frequency and mode shape," *Journal of Applied Mechanics* 47(2):461, 1980.

[10] Leissa, A.W., "Vibration of Shells," Scientific and Technical Information Office, National Aeronautics and Space Administration, 1973.

[11] Gelman, A., Carlin, J.B., Stern, H.S., and Rubin, D.B., "Bayesian data analysis," Chapman and Hall/CRC, ISBN 0-429-25841-0, 1995.

[12] Vehtari, Aki, and Janne Ojanen. "A survey of Bayesian predictive methods for model assessment, selection and comparison." (2012): 142-228.

[13] Martin, Osvaldo A., Ravin Kumar, and Junpeng Lao. Bayesian Modeling and Computation in Python. CRC Press, 2021.